An *ab initio* Hartree–Fock study of α-MoO_3

Furio Corà,*[a] Atul Patel,[a]† Nicholas M. Harrison,[b] Carla Roetti[c] and C. Richard A. Catlow[a]

[a]*The Davy Faraday Research Laboratory, The Royal Institution of Great Britain, 21 Albemarle Street, London, UK W1X 4BS*

[b]*TCS Division, Daresbury Laboratories, Daresbury, Warrington, UK WA4 4AD*

[c]*Dipartimento di Chimica Inorganica, Chimica Fisica e Chimica dei Materiali, Università di Torino, Via Giuria 5, I-10125, Italy*

The structural and ground-state electronic properties of the layered orthorhombic molybdenum trioxide (α-MoO_3) have been investigated using a periodic boundary condition *ab initio* Hartree–Fock method. The effect of electron correlation is estimated with *a posteriori* density functional corrections to the total energy. The structure has been optimised using the correlation corrected Hartree–Fock energy (except for the interlayer separation where the correlation correction has not been applied), treating each degree of freedom independently. The bonding in the solid is examined in detail: the nature of the Mo—O interaction changes considerably with the equilibrium bond distance, and varies from strongly covalent for the shortest bond to a predominantly ionic interaction for the longest bonds in the MoO_6 octahedron. The degree of covalence in the bonding is characterised using electron density maps and the Mulliken population analysis; the net charge shows a value as low as $-0.44|e|$ for the oxygen involved in the shortest Mo—O bond. The energy as a function of the interlayer spacing has a minimum, both at the correlated and the Hartree–Fock level, indicating that a weak attractive Coulombic force is active between adjacent layers.

The properties displayed by the molybdenum oxides, and their several fields of application are attracting a growing interest in these materials. In particular, MoO_3 is an important heterogeneous catalyst component, both when used alone and when activated on a suitable oxidic support. Industrial applications are found in the fuel industry in the processes of hydrocracking[1] and desulfurization;[2] in the de-NO_x,[3] partial oxidation[4] and metathesis[5] reactions, and also in the manufacture of synthetic fibres, specifically in the production of the monomer maleic anhydride.[6] However, interest in this compound extends beyond its catalytic behaviour: its electro/photochromic properties are being exploited for solar cell technology,[7] and the nanostructural material could be useful in developing mechanical logic gates.[8] MoO_3 is also the parent oxide for the molybdenum bronzes, a class of insertion compounds which exhibit novel and useful electronic properties, in particular large anisotropies in the electrical conductivity with respect to the crystal planes, metal-to-semiconductor transitions *via* Peierls distortions and charge density waves.[9]

Molybdenum trioxide at ambient conditions is present in two polymorphs: the ReO_3 structured β-MoO_3[10,11] and the layered α-MoO_3. Both are built up from octahedral MoO_6 structural units, but the three-dimensional connectivity of the octahedra differs. The structure of β-MoO_3 is a common arrangement in the solid-state chemistry of transition-metal trioxides, and has an equivalent in binary ReO_3[12] and WO_3;[13] it is based on a network of corner-sharing octahedra where all the oxygen ions are in a two-fold coordinated bridging position between adjacent metal sites. The crystal structure of α-MoO_3 was first determined in 1931 by Brakken[14] and Wooster;[15] both studies found that the trioxide could be described as a layered orthorhombic arrangement with space group *Pnma* and four formula units of MoO_3 per unit cell. Kihlborg refined the structure,[16] showing that the MoO_6 octahedra are considerably distorted around the metal centre, with a spread of the Mo—O bond distances which range from 1.67 to 2.34 Å (see Fig. 1). The experimental parameters are reported in Table 1. The layered disposition of octahedra found in α-MoO_3 is unique to molybdenum trioxide, and its equivalent has not been observed in other oxides. In the crystal structure of α-MoO_3 we can identify a preferential direction (*a*), perpendicular to the layers, along which the octahedral units are not connected to one another; within the layers the connectivity of the MoO_6 octahedra occurs in one direction (*b*) by common edges, so as to form zigzag rows, and in the perpendicular (*c*) by common corners only. A schematic picture of the structure is displayed in Fig. 1(*a*) and (*b*). The anisotropy in the connectivity between MoO_6 octahedra results in a different local environment for the oxygens, that are now topologically inequivalent. The outermost oxygen in each layer [labelled O(1) in Fig. 1] has only one nearest molybdenum atom; where the octahedra are connected by corner-sharing, the oxygens [O(2) in Fig. 1] are two-coordinate, as in β-MoO_3, while oxygens along shared edges are three-coordinate [O(3) in Fig. 1]. In the coordination octahedron around each molybdenum atom [Fig. 1(*c*)], one oxygen is of type O(1), two are of kind O(2) and three

Table 1 The optimised structure of α-MoO_3 compared to experimental data[a]

structure parameter	calc.	obs.[16]	structure parameter	calc.	obs.[16]
a/Å	14.271	13.855	O(2) (*z*)	0.5182	0.5212
b/Å	3.680	3.696	O(3) (*x*)	0.4417	0.4351
c/Å	3.910	3.963	O(3) (*z*)	0.5124	0.4994
V/Å^3	205.34	202.94	Mo—O(1)/Å	1.643	1.671
Mo (*x*)	0.0956	0.1016	Mo—O(2)/Å	1.687	1.734
Mo (*z*)	0.0887	0.0867	Mo—O(2′)/Å	2.237	2.251
O(1) (*x*)	0.2113	0.2214	Mo—O(3)/Å	1.937	1.948
O(1) (*z*)	0.0483	0.0373	Mo—O(3′)/Å	2.212	2.332
O(2) (*x*)	0.0841	0.0866			

[a]The index used for labelling the oxygen atoms refers to their coordination in the crystal structure; oxygens with same coordination number, but at a different distance from the Mo ion in the MoO_6 coordination octahedron have been labelled with a prime

† Present address: The Research School of Geological and Geophysical Science, University College London, Gower Street, London, UK WC1E 6BT.

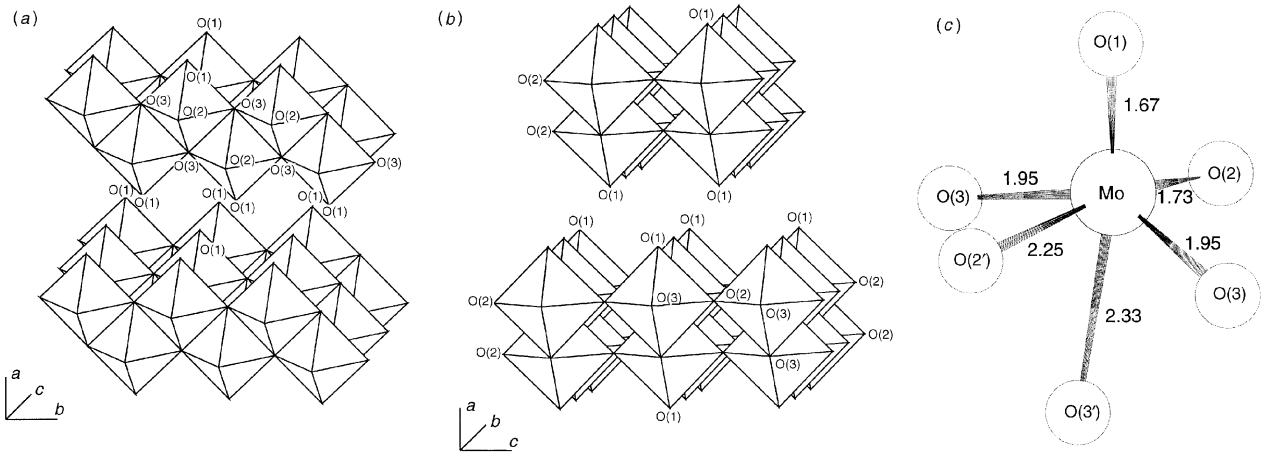

Fig. 1 Structure of α-MoO_3. (*a*), (*b*) Network of edge- and corner-sharing MoO_6 octahedra, showing the layered structure of α-MoO_3 and the layer orientation relative to the lattice vectors of the solid. Oxygen octahedra are connected corner-sharing along the *c* crystallographic axis and edge-sharing along the *b* direction. (*c*) Distorted MoO_6 octahedron highlighting the distribution of bond lengths (in Å) as obtained from the experimental refinement.[16]

are O(3). The local atomic environment of the two polymorphs of MoO_3, therefore, differs more with respect to the oxygens, rather than to the metal atom.

The fundamental solid-state chemistry of the perovskite-like structure of β-MoO_3 has been investigated theoretically with extended-Hückel,[17] and more recently with *ab initio* calculations.[18–20] In this paper we apply *ab initio* methods of the same quality as employed in ref. 18 to investigate the chemical properties of the layered α-MoO_3 phase. Due to the unique crystal structure and to the many industrial applications referred to above, α-MoO_3 is an interesting material to study using theoretical techniques. Only one previous quantum mechanical study of this solid has been reported, which predicted the XANES absorption spectra of the Mo atom in the trioxide as well as $NiMoO_4$.[21] In the present study we will attempt to optimise the structure, characterise the chemical bonding and investigate the ground-state electronic properties of α-MoO_3. Finally, we will compare the chemical features of the two polymorphic, α and β, structures.

Computational method and basis set

The computational model that we have employed to study the bulk material is based on periodic boundary conditions, at the *ab initio* Hartree–Fock (HF) level of approximation, as implemented in the code CRYSTAL.[22,23] The wavefunction of the solid is described in terms of crystalline orbitals; these are obtained as linear combinations of localised functions, or atomic orbitals (AOs), associated with atomic positions.

The approximations in such an approach are of two kinds: methodological and numerical. The neglect of electron correlation, intrinsic to the HF theory, is ascribed to the first class. In the following sections the HF results have been corrected using a correlation energy, which is calculated *a posteriori*, with a density functional of the HF density, according to the generalised gradient approximation (GGA) scheme proposed by Perdew *et al.*[24,25] However, no correction has been attempted for the HF wavefunction.

Numerical approximations are introduced in the implementation of the self-consistent field (SCF) equations for an infinite system. The accuracy in the evaluation of the infinite Coulomb and exchange series is controlled by a set of 'cut-off' thresholds (see ref. 22 for details); in the present case we have chosen a set of very severe computational tolerances (8, 7, 8, 8, 16), to reduce the effect of numerical inaccuracies to a minimum. Reciprocal space integrals are performed by sampling the first Brillouin zone at a discrete set of equispaced *k*-points, that define the Pack–Monkhorst net.[26] In the geometry optimisation we have used 27 irreducible (64 total) *k*-points; selected final calculations have been repeated with an improved grid (75 irreducible, 256 total *k*-points), that gives well converged results in the numerical integration.

The final limitation of our approach is related to the finite size of the variational basis set. Because of the large number of electrons (*i.e.* 42) in the molybdenum atom, we have used a small-core effective-core pseudopotential (ECP) of the Hay–Wadt type[27] which accounted for the electrons $1s^2$–$3d^{10}$. The valence basis set for molybdenum is composed of 22 AOs; using the notation adopted by Hehre *et al.*,[28] the molybdenum basis set is 311-31G. The oxygen basis set is a 8-51G, optimised for MgO in a previous study,[29] which has already been used in several other oxides.[18,30,31] The molybdenum basis set has been developed from the atomic solution and further refined by optimising the exponents and contraction coefficients of the d orbitals. We note that all the basis set optimisations were performed with respect to the HF energy in the cubic structure of the β phase, whose geometry has been chosen in such a way that the volume per formula unit is the same as in the experimental geometry of the monoclinic phase;[10,11] the resulting lattice parameter was $a = 3.76$ Å. We recall that the local environment of the Mo atom is similar in both polymorphs, and the high symmetry of the ReO_3 structure made the optimisation less computationally demanding. The molybdenum basis set employed in the computations is given in Table 2. Basis sets of this quality have proved adequate to describe most crystalline materials;[23] the presence of unoccupied AOs on both oxygen and metal gives flexibility to the

Table 2 The Mo^{6+} basis set employed in the calculations. The core electrons ($1s^2 2sp^8 3sp^8 3d^{10}$) are described by a Hay–Wadt type, small core ECP[27]

		coefficient	
shell type	exponent	s	p or d
4sp	12.0795	0.01275	−0.01618
	2.6745	−0.86046	−0.30674
	1.5970	0.77399	0.65206
5sp	0.6300	1.00000	1.00000
6sp	0.1900	1.00000	1.00000
4d	1.6630		0.09700
	1.0830		0.24100
	0.3570		0.53000
5d	0.2200		1.00000

basis, and allows the polarizability of both species, and back-donation effects from the oxygens to the metal to be taken into account.

Results and Discussion

Structural analysis, geometry optimisation and energetics of α-MoO_3

Ideally, one would like to optimise the crystal structure completely. For a system with many degrees of freedom (11 for orthorhombic α-MoO_3), however, this is very computationally expensive; on the other hand, once all the major chemical and physical features of the solid are correctly represented, small geometry modifications do not alter appreciably the overall description obtained for the material. For this reason, we have employed the following simplified strategy in the geometry optimisation: we first analyse the solid, and identify the basic structural components, such as the layer orientation, covalent groups, bond lengths and angles, and assess their relative importance in the energetics of the interaction. The internal coordinates of the structural components are then varied one at the time, in order of decreasing bond strength involved. Once the coordinates corresponding to the minimum energy have been found for one degree of freedom, the geometry of that component is fixed at its optimum value, and not modified further. In doing so we implicitly assume that on relaxing the degrees of freedom corresponding to the weakest interactions in the solid, the equilibrium geometry due to the stronger forces is not appreciably influenced. This procedure is justified if the difference in the bond strength involved in different structural components is sufficiently high; we will later check and comment on the accuracy of this choice *a posteriori*, in the discussion in the following sections.

Guidance as to understanding the relative energetics of the different structural components is provided by simple structural and chemical considerations; we also refer to the results of our previous study of the isoelectronic, and chemically similar oxide, WO_3.[18] We showed in that work that the most important component of the bonding in the solid is the electrostatic attraction between metal and oxygens complemented by a strong, but localised, covalent contribution between the metal and one particular oxygen. The equilibrium distance of the covalently bound W—O pair in tetragonal WO_3 is considerably shorter than all the other W—O bond lengths; in ref. 18 we also found that the covalent W—O group was only marginally affected by modifications in the overall crystal structure. For example, a 10% change in the volume per formula unit resulted in a change in the shortest bond length of only 0.18%. It is legitimate therefore to identify the bonded W—O pair as a single unit, or tungstyl group. The experimental evidence, from the spread of Mo—O bond distances in α-MoO_3,[16] suggests that similar behaviour is observed also in molybdenum oxide.

To start our analysis of the bonding, we perform an initial factorisation of the problem, as suggested by the layer structure of α-MoO_3, which allows us to consider separately the intra- and inter-layer interactions.

Let us consider first the intralayer forces. Here, we need to decide which oxygen is more likely to have the strongest interaction with the molybdenum atom. To this end, we have examined the local environment of each species, taking into account the differences in the Mo—O bond lengths and the inequivalence of the oxygens. The shortest experimentally observed Mo—O distance involves O(1), which is attributable to two factors. First, O(1) is the species with the lowest coordination in the crystal structure. We know that the fully ionic state of oxygen, with the formal charge of −2, is stabilised in the solid state by the field created by neighbouring cations, but that O^{2-} is unstable when isolated. Therefore, since O(1) has the lowest coordination number, it has the highest tendency towards a covalent interaction with the metal. The second factor is evident when we note that each layer in the solid is terminated with a stratum of O(1) atoms (see Fig. 1), and in the interlayer region O(1) atoms face one another. The electrostatic repulsion can be lowered by a reduction in the ionic charge of these atoms, as can be obtained in practice by increasing the Mo—O(1) covalence, so that electrons are delocalised towards the metal and are drawn away from the oxygen. The combination of the two effects above is such that we expect a very strong and covalent interaction between Mo and O(1), in agreement with the very short bond length observed in ref. 16. A similar argument to that employed for O(1) can be used to differentiate the properties of O(2) and O(3); we expect in fact that an increase in the coordination number of the oxygen corresponds to an increase in its ionicity. The two-coordinate O(2) should therefore give a more covalent and stronger bond with Mo than the three-coordinate O(3). The analysis can be further validated by examining the *trans*-effect of the oxygen ligands around the Mo atom. It is well established in coordination chemistry that the stronger a bond in a square-planar complex, the weaker is the one in the opposite (*trans*) direction with respect to the central metal.[32] The explanation is due to the competition of *trans* ligands for the same set of AOs on the metal. Based on simple symmetry requirements, this concept can be extended to octahedral complexes, both in molecular species and in the solid state; the influence of the *trans*-effect on MO_6 octahedra in solid-state chemistry agrees both with extended-Hückel results[17] and with our previous HF calculations on WO_3. *trans* to the strongly bound O(1) atom in α-MoO_3 we find an O(3) species, which is therefore expected to provide the weakest interaction in the MoO_6 octahedron.

All the previous arguments concur to define the following order in the intralayer interaction energies: Mo—O(1) > Mo—O(2) > Mo—O(3). This analysis is in agreement with the experimentally determined bond lengths.

Let us now move to analysing the forces holding the layers together. We note here that each layer is symmetry equivalent and charge-neutral, and we can therefore exclude strong ionic forces. Moreover, since changing the interlayer spacing does not involve changing any of the nearest-neighbour Mo—O distances, we expect that the interlayer bonding represents a weak interaction. In previous studies on similar layered structures [for example β-$MgCl_2$[33,34] and $Mg(OH)_2$[35]] it was found that the layer–layer interaction was very weak indeed, and limited to dispersive forces. Other molybdenum-based layered compounds, in particular MoS_2,[36] are used in industry as lubricants owing to their easy cleavage and low interlayer forces. This is not the case, however, for MoO_3, for which we might expect a stronger interaction. We analyse the interlayer bonding in greater depth in the next section, using the calculated electronic distribution. At this stage we simply note that the interlayer bonding is weaker than the intralayer interactions. We have therefore obtained the desired scale of interaction energies, according to which we can perform our simplified geometry optimisation, as proposed earlier in this section.

The starting point for the optimisation is the experimental geometry, as derived from ref. 16. Following the previous discussion, we have first of all optimised the intralayer structure and then subsequently the interlayer spacing. The first parameter in the intralayer geometry optimisation was the short Mo—O(1) bond length; this degree of freedom was varied and then fixed at its optimum value of 1.644 Å; subsequently the baricentre of the Mo—O(1) couple was shifted within the MoO_6 octahedron, and anchored at its minimum energy position. Next we considered the Mo—O(2) interaction, and optimised the coordinates of the O(2) species with respect to the rest of the crystal; the above optimisation yields an

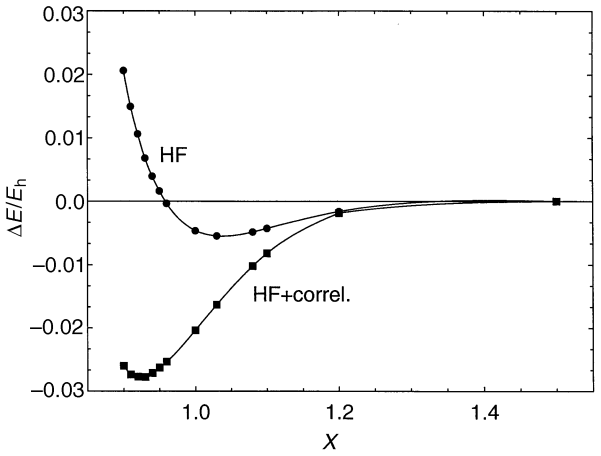

Fig. 2 Plot of the optimisation of the interlayer spacing. The scaling parameter X is defined in the text; $X=1.0$ for the experimental structure. The two lines refer to the HF results and to the correlation-corrected values, as indicated.

Mo—O(2) optimum distance of 1.710 Å, which is short enough to provide a strong interaction energy, but sufficiently longer than the Mo—O(1) distance to validate our initial hypothesis. The x and z fractional coordinates of O(3) were the last of the oxygen parameters to be optimised. At this point we scaled the b and c lattice parameters, to obtain the resulting equilibrium intralayer structure. Subsequently, the layer geometry is kept fixed, and the layer–layer separation allowed to vary.

The interlayer spacing is a difficult parameter to define unambiguously; we make reference to the lattice parameter a, which defines the direction perpendicular to the layer orientation in the solid. In the space group *Pnma*, the layers in each unit cell are centred at the positions with fractional coordinates $x=0.0$, $x=0.5$ and $x=1.0$. The layer at $x=0.5$ is translated half a lattice vector along the b and c directions with respect to the layers at $x=0.0$ and $x=1.0$. To change the interlayer spacing we have applied a scaling factor X to the lattice parameter a, balanced by a factor $1/X$ for the distance (in internal coordinates) of each atom from the baricentre of its layer. This operation leaves the intralayer structure unaltered, but varies the distance of the baricentre of adjacent layers by a factor X. We note that the experimental value of $a=13.855$ Å corresponds to a scaling factor $X=1.0$. Fig. 2 shows a plot of the relative energy against the scaling factor X thus defined, at both the HF and correlated levels of theory. In both cases the zero of energy has been chosen as coincident with the energy of the structure with the highest interlayer separation, which corresponds to $X=1.50$.

The optimised geometry obtained is compared to the experimentally determined structure[16] in Table 1. The agreement is in general good; bond distances are slightly underestimated in our calculations, but this is a general result for GGA-corrected HF values. We can now focus on the calculated equilibrium geometry, and perform a quantitative analysis of the forces involved in the solid, which will also provide us with a validation of the qualitative assumptions made in the geometry optimisation.

From the quantum-mechanically derived electronic distribution in the solid, we can perform several analyses: electron density maps and profiles, population analyses, electrostatic potential maps, band structures and projected densities of states (PDOS). In the following discussion we make use of these tools to extract a wide range of information for the solid. In analysing the results we preserve the factorisation of the problem into intra- and inter-layer interactions.

Electronic structure and bonding of α-MoO_3: intralayer

When examining the intralayer forces, our main interest is to analyse the short-range (chemical) interaction between the central molybdenum atom and its six nearest-neighbour oxygen ligands that form the octahedral building unit of the solid. Fig. 3 reports a contour plot of the difference electron density for the optimised geometry. The map is obtained by subtracting the density of isolated Mo^{6+} and O^{2-} ions from the total electron density of the solid. The former represent an ideal ionic description of the solid, where no covalence is included; moreover they are spherical species and represent an appropriate reference to highlight the chemical features of the electronic distribution in the solid. The density of the isolated ions is obtained by solving the HF equations for the ions, using the same basis set as employed in the solid-state calculation; due to the finite size of the basis set, the HF calculation on the O^{2-} ion converges, and the density of the isolated ion can be defined. With reference to the labelling of atoms reported in Table 1, the plot of Fig. 3 is drawn in the crystallographic *ac* plane, and cuts the MoO_6 octahedra in a slice containing the Mo ion at the centre, and the O(1)O(2)O(3′)O(2′) vertices; the window chosen is long enough to include some of the interlayer space (region A in the figure). The anisotropy in the bonding is quite evident in the map; in particular, we note that the two short bonds Mo—O(1) and Mo—O(2) display a significant increase of charge density in the bonding region typical of covalent interactions, which is not present in the longer Mo—O(3′) and Mo—O(2′) bonds.

To pursue the investigation of the degree of covalence in each of the Mo—O bonds it is, however, necessary to quantify the information given graphically in Fig. 3. In order to do so,

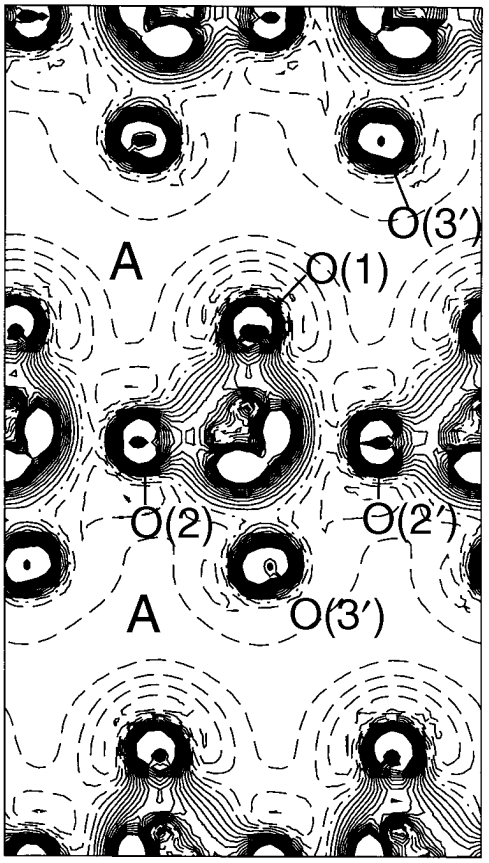

Fig. 3 Difference electronic charge density map (solid minus isolated Mo^{6+} and O^{2-} ions), displayed in the crystallographic *ac* plane, containing the central Mo and the vertices O(1)O(2′)O(3′)O(2) of one MoO_6 octahedron. Continuous, dashed and dot-dashed lines correspond to positive, negative and zero difference respectively. The interval between the isodensity lines is 0.005 a.u. (electrons a_0^{-3}). The map extends beyond the central octahedron, and includes part of the interlayer space, denoted by A.

we have used a Mulliken population analysis of the electronic distribution. Results within the coordination octahedron are summarised in Table 3. The picture that arises from the data is quite clear: the net charge on the Mo ion is large enough to give a strong ionic contribution to the bonding; covalence effects contribute to decrease the net charge on the metal by transferring (back-donating) electrons from the oxygens. The net charge on the non-symmetry-equivalent oxygens gives unambiguous information regarding the nature of the interaction: O(1) has a strikingly low value for an oxide species, being as low as $-0.44|e|$. This value is half the (already low) net charge on O(2) of $-0.75|e|$, and a third of the net charge on O(3) of $-1.25|e|$. The degree of covalence of the bonds is confirmed by the bond population analysis, reported in the last column of Table 3: the short Mo—O(1) bond has a population $q_b = 0.29|e|$, which is very high. The corresponding value of q_b for the Mo—O(2) bond decreases sharply to $0.10|e|$, indicating, however, that covalence in the bonding is still appreciable. All other bonds have a negative overlap population, which excludes major covalent contributions to the bonding. This quantitative analysis is in excellent agreement with the analysis given in the previous section.

To stress further the anisotropy of the bonding, we report in Fig. 4 the electron density profile along the six Mo—O bonds. As in Fig. 3, we have obtained the value by subtracting the ionic contribution of Mo^{6+} and O^{2-} species from the total electron density in the solid. In Fig. 4, the Mo atom is at the origin of the x axis, and the abscissa refers to the Mo—O distance. Fig. 4 shows a very strong dependence of the electronic redistribution on the bond length. The accumulation of electron charge in the internuclear region, which characterises covalent bonds, is clear for the short Mo—O bonds, while for the longer bonds we observe a polarisation of the ions, but the electronic charge is close to the atomic centres and therefore must be attributed to the ions, rather than shared in the central region. On decreasing the equilibrium distance, there is an increasingly pronounced redistribution of charge towards the centre of the bond.

The present result, combined with the Mulliken population analysis reported above, suggests that oxygens with a different coordination number behave as truly different chemical species in α-MoO_3.

It is instructive to compare the present results for α-MoO_3 with our previous calculations on WO_3.[18] The two solids are isoelectronic and chemically very similar. Calculations on both compounds have been performed using exactly the same computational conditions, and results can therefore be compared directly. For completeness, in the lower part of Table 3we report our results relating to bond distances and Mulliken population analysis for tetragonal and cubic WO_3. It is

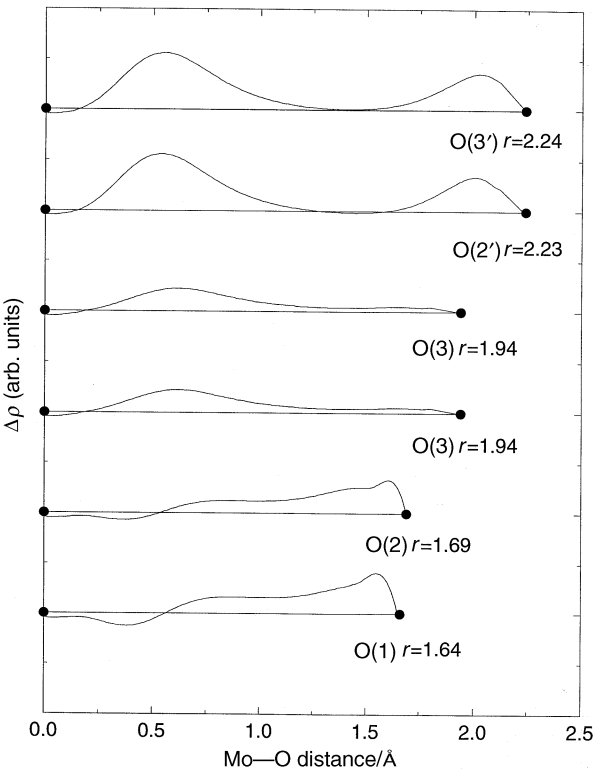

Fig. 4 Difference charge density profiles, $\Delta\rho$ (relative to Mo^{6+} and O^{2-} ions), along each Mo—O bond. Black circles indicate the position of the atoms: Mo on the left, O on the right. The horizontal lines represent the zero difference charge density for each bond.

important to note the different structure and symmetry of the two solids examined: WO_3 has a distorted ReO_3 structure, while α-MoO_3 is layered; in our work on WO_3 we had considered higher symmetry phases, in which the central metal ion was at the centre of its coordination octahedron (cubic), or displaced towards one oxygen ligand only (tetragonal); in the orthorhombic phase the metal is displaced instead towards two oxygen ligands. These are important factors, and must be taken into due account when comparing the two phases.

The general trend that emerges from Table 3 confirms the similarity in the chemical behaviour of tungsten and molybdenum trioxides. In both cases the metal forms a very strong covalent bond with one particular oxygen ligand [labelled O(1) in Table 3 for both α-MoO_3 and tetragonal WO_3]. In both solids M—O(1) is a very strong bond, and by analogy with the WO_3 results, we identify the Mo—O(1) pair in α-

Table 3 Equilibrium bond distances and Mulliken population analysis for α-MoO_3 and WO_3 (from ref. 18). The entry labelled as $\langle O \rangle$ refers to the average M—O value in a MO_6 octahedron

	atom	multiplicity	net charge/e	bond distance r(M—O)/Å	bond population q_b(M—O)/$\|e\|$
α-MoO_3 (orthorhombic)	Mo		+2.43		
	O(1)	1	−0.44	1.643	+0.29
	O(2)	1	−0.75	1.687	+0.10
	O(3)	2	−1.25	1.937	−0.02
	O(2′)	1	−0.75	2.212	−0.02
	O(3′)	1	−1.25	2.237	−0.00
	$\langle O \rangle$	6	−0.81	1.942	+0.055
WO_3 (cubic)	W		+4.09		
	O	6	−1.36	1.883	−0.03
WO_3 (tetragonal)	W		+3.79		
	O(1)	1	−0.97	1.629	+0.21
	O(2)	4	−1.41	1.895	−0.01
	O(1′)	1	−0.97	2.366	−0.00
	$\langle O \rangle$	6	−1.26	1.929	+0.03

MoO_3 as a molybdenyl group. The further symmetry lowering from tetragonal to orthorhombic brings the metal closer to a second oxygen ligand [O(2)], with which there is a covalent interaction, but to a much lesser extent than with O(1). The overall interaction between molybdenum and oxygen appears to be more covalent than between tungsten and oxygen, which is confirmed by the lower ionic charges and higher bond population (q_b) values in MoO_3 compared to WO_3. The first reason for the different behaviour is chemical: Mo is above W in group VI-A of the Periodic Table, and its AOs are more compatible (*i.e.* closer in energy) with the oxygen levels than are the W orbitals; in more classical terms, Mo is slightly more electronegative than W. The second reason is structural: as shown in the previous section, the lower coordination of O(1) in α-MoO_3 makes it more prone to covalent interactions than the local environment of O(1) in tetragonal WO_3. We are not able, however, to quantify the relative importance of these two effects using the data available from this study.

To complete the characterisation of the intralayer forces, in Fig. 5 and 6 we report the band structure and the PDOS of the solid, respectively. We observe three main features, which can be characterised as the oxygen 2s (in the region of -1.25 E_h in Fig. 6), the valence band, with contributions from both oxygens and molybdenum (-0.5 E_h), and the conduction band (starting at 0.1 E_h). The calculated band structure confirms that α-MoO_3 is an insulator with a band-gap at the Γ point of 0.45 E_h (12.4 eV). However, the HF approximation is known to overestimate the band-gap, sometimes by a factor of 2 or more.[37] The gap in α-MoO_3 is considerably higher than 8.1 eV calculated for tetragonal WO_3,[18] known experimentally to be a semiconductor.[38] The higher band-gap is consistent with a stronger covalent character in the M—O interaction.[39]

From inspection of the total and projected density of states (PDOS), we find that the different oxygen atoms have distinct, but similar PDOS in the valence region. The valence band appears to be composed of two sub-bands: the one at higher energy (*i.e.* the highest peak in Fig. 6, just below the Fermi energy) has contributions from the oxygen atoms, but a very small component on the metal. This is a common feature of the PDOS that was obtained also in WO_3,[18] ReO_3 and $NaWO_3$.[19,20] We attribute this sub-band to the unshared electron pairs on the oxygen ions; the corresponding bands in Fig. 5 are very flat in k-space. The lower sub-band has, in contrast, appreciable contributions from both oxygen and metal; it therefore accounts for the chemical interactions in the solid. The corresponding bands show a more appreciable dispersion in k-space. Effects of this kind have been examined extensively with extended-Hückel methods,[17] and are typical of covalent interactions. The low symmetry of the phase examined makes it impossible to separate single contributions to the bonding without employing localisation techniques for the electrons, such as Wannier functions, that unfortunately are not currently implemented in the code we have employed.

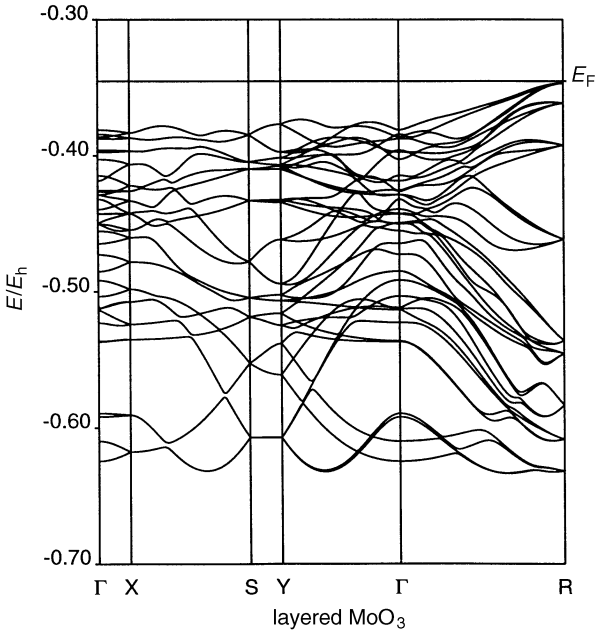

Fig. 5 Valence band structure for α-MoO_3 in a typical orthorhombic reciprocal space path, including all the high-symmetry positions of the first Brillouin zone

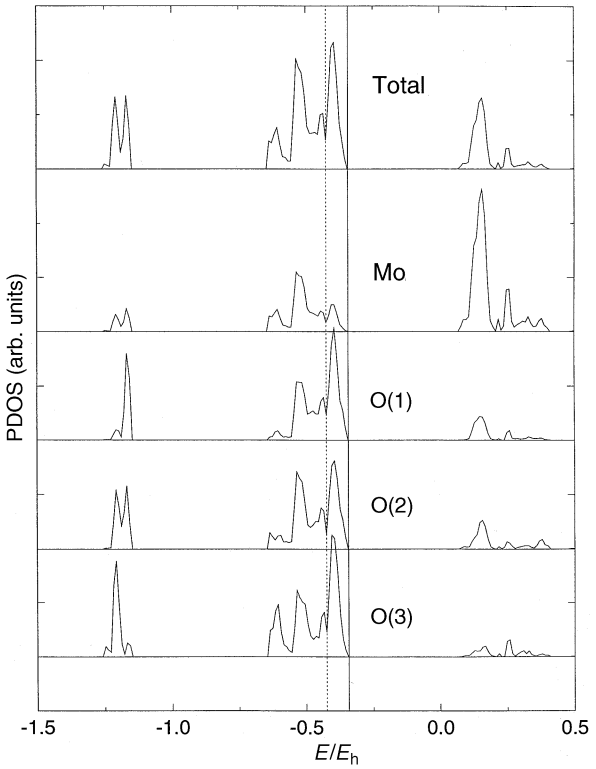

Fig. 6 Projected density of states (PDOS): total value for the solid, and contributions from symmetry-unique atoms. The continuous vertical line marks the Fermi energy position (top of the valence band); the dotted vertical line highlights the presence of two sub-bands, as mentioned in the text.

Electronic structure and bonding of α-MoO_3: interlayer

In Fig. 2 we report the energy change due to the variation of the interlayer spacing of the solid, as a function of the scaling parameter X defined in the previous section, both at the HF and at the correlated level. The interlayer binding energy is 0.0055 E_h (0.15 eV) per unit cell at the HF level, and rises to 0.0278 E_h (0.75 eV) on including correlation.

It is interesting to note that the HF approximation alone can provide a minimum energy position, although the equilibrium interlayer spacing ($X = 1.04$) is slightly overestimated with respect to the experimental value (corresponding to $X = 1.00$). The forces included at the HF level of theory arise from Coulomb and exchange terms, but the dispersion (van der Waals) contribution to the bonding is excluded. This result shows therefore that in α-MoO_3 long-range interactions contribute to the interlayer bonding. In this respect the behaviour of α-MoO_3 is different from that of the previously studied layered solids [β-$MgCl_2$[33,34] and β-$Mg(OH)_2$[35]] where the layer–layer interaction was found to be due only to dispersion forces, which had to be included in the model either *ad hoc*, with a semiclassical contribution,[33] or *via* the *a posteriori* correlation correction to the HF energy.[34,35]

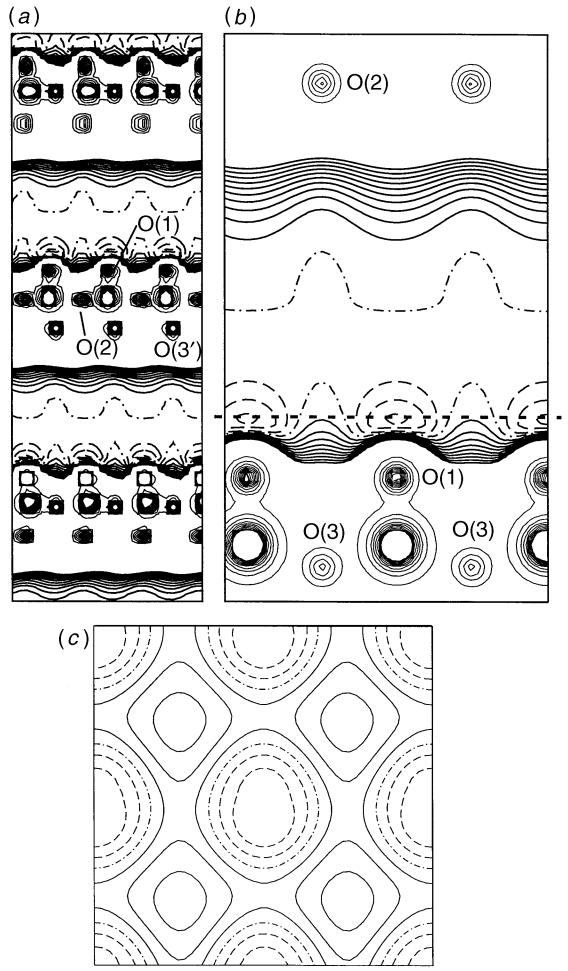

Fig. 7 Electrostatic potential map in the crystallographic (*a*) *ac*, (*b*) *ab*, and (*c*) *bc* planes. The window sizes used are different in the three cases: (*a*) includes three adjacent layers to highlight the long-range structure of the solid; (*b*) is drawn between the centre of mass of two adjacent layers, and provides a better resolution of the electrostatic potential in the near-layer region; (*c*) shows the alternation of regions of positive and negative potential above each layer. In (*a*) and (*b*) the isopotential lines in the intralayer region represent the atomic coordinates in the layers; atoms are labelled as in Fig. 1. Continuous, dashed and dot-dashed lines correspond to positive, negative and zero potential respectively. The interval between isopotential lines is 0.005 a.u. (1 a.u. = −27.21 V), as described in the text. The dashed line above the outermost oxygens in (*b*) represents the projection of the plane in which plot (*c*) is drawn.

To investigate further the contribution of long-range interactions to the layer–layer bonding, we show in Fig. 7 three maps of the electrostatic field created by the electronic and nuclear distribution of the solid, in mutually perpendicular planes. To clarify these representations, we have increased the layer–layer separation (the maps correspond to a scaling factor $X=2.0$), so that the field created by adjacent layers does not overlap. Fig. 7(*a*) and (*b*) are created by the superposition of two plots: each layer is in fact charge-neutral, and the Coulomb field projecting outside the layers has a low value. To gain resolution in the interlayer region, in the first plot we have used a low difference between isopotential lines (0.005 a.u.; 1 a.u. = 27.21 V), and a very low cut-off threshold of ± 0.05 a.u. The potential in the intralayer space is higher than the cut-off value, and most of the intralayer space in the first plot is blank. To mark the atomic positions, we have superimposed a second plot, comprising the isopotential lines between 2 and 10 a.u. at steps of 1 a.u.; the zones marked in the second plot correspond to the maxima of the electrostatic potential in the respective planes, and are located in the near-nuclear region. Atoms are labelled here as in Fig. 1. The plane in which Fig. 7(*a*) is drawn is that defined by the crystallographic *a* and *c* axes; Fig. 7(*b*) is drawn in the *ab* plane, instead. The former is the same plane employed to draw the electron density map of Fig. 5. In the space group *Pnma*, the glide plane '*a*' translates each layer of $\{\pm 0.5a \pm 0.5b \pm 0.5c\}$ lattice vectors; referring to the planes of Fig. 7(*a*), (*b*), each layer is therefore repeated, but translated by half a lattice vector along the direction perpendicular to the map. Although of low intensity, we note that the electrostatic potential created by each layer is non-zero in the near-layer region. In particular a negative contribution prevails in the region above the outermost oxygens, O(1), and a positive contribution where octahedra connect by corner-sharing, in the region above the O(2) species.

Map 7(*c*) illustrates how positive and negative zones connect above each layer; the plane employed there is parallel to the layer orientation (the *bc* crystallographic plane), and lies at 8.0 a_0 above the centre of mass of the layer [2.3 a_0 above the O(1) nuclear position]; its projection is marked with a dashed line in Fig. 7(*b*). We clearly see in Fig. 7(*c*) that the potential created by the layer forms a pattern of positive and negative areas, similar to the (001) surface of MgO. The negative zones are above O(1) atoms; the positive zones correspond to the O(2) and O(3) regions. Under the effect of the glide vector '*a*', in the next layer the same pattern is repeated, but translated by half a lattice vector along *b* and *c*, so that positive areas are translated above the negative ones. At the equilibrium interlayer separation, positive and negative zones in adjacent layers overlap, thus giving a non-zero Coulombic contribution to the HF binding energy, as noted when discussing Fig. 2.

A possible reason why this electrostatic interlayer bonding is present in α-MoO_3 but not in β-MgX_2 is the lower symmetry of the former phase, which is due both to the coordinates of the metal ion, that are considerably off-centre in its coordination octahedron, and to the inequivalence (in particular in the ionic charge) of the different oxygens. The low symmetry has the major consequence that the Coulomb field does not perfectly balance in each MoO_6 octahedron, resulting in a medium-range component for the electrostatic field acting between adjacent layers.

The slope of the curve of Fig. 2 is significantly altered when the correlation corrections are added to the HF energy, which means that dispersive forces still play an important role in the interlayer bonding in α-MoO_3. The minimum of the corrected HF energy corresponds to $X=0.93$, which is considerably lower than the experimental spacing. It must be noted, however, that the interlayer interaction is indeed weak, and even a small overestimation of the van der Waals contribution can cause a large error in the equilibrium geometry (though not in the binding energy). We comment further on this topic in the analysis of the density maps in the interlayer region.

Given the weak interlayer forces, the (100) planes, that define the layer orientation in the solid, represent an easy cleavage direction for the material; and in light of these results, we expect that most of the surfaces exposed by an α-MoO_3 crystallite will be of (100) type. For the same reason, we consider that the potential which we have plotted in Fig. 7 will be very similar to the electrostatic potential generated by a free α-MoO_3 (100) surface. The result obtained here encourages therefore extensions of the present study to the α-MoO_3 surfaces and to the adsorption processes thereon.

We need also to consider in greater detail the interlayer region (labelled A) in the difference density map of Fig. 3. We note in this respect the negative contribution around the outermost atoms in each layer, in particular around O(1). We recall that the map is obtained by subtracting the density of the isolated ions from the total density of the solid; the higher the negative contribution, the more the ions in the solid are contracted. The contraction effect is most pronounced for O(1): as noted earlier, O(1) species are facing one another in

the interlayer region. By decreasing the effective radius of O(1), the two-body repulsion between layers is effectively reduced, just as the electrostatic repulsion between layers is reduced by decreasing the ionic charge of O(1).

The molybdenyl Mo—O(1) groups in adjacent layers are connected to one another in a zip-like manner. To focus on this structural feature, we have plotted the difference electron density map (with the same reference and conventions used in Fig. 3) in the plane passing through the terminal molybdenyl groups in the interlayer region; the result is shown in Fig. 8. The contraction of the O(1) electronic cloud, as well as the short O(1)···O(1) distance (about 2.7 Å, depending on the interlayer separation) are immediately apparent from Fig. 8. The short O(1)···O(1) distance, as well as the low net charge of O(1) suggest that in some circumstances, adjacent O(1) species belonging to different layers could bind to form a superoxide (O_2^{2-}) unit. In all our calculations, however, the bond population between nearest neighbour O(1) species was negative, a result which seems to exclude the possibility of superoxide units, at least in the ground electronic state of the material. It is possible, however, that the presence of superoxide type bonds between O(1) species could represent a common defect in this material. If this were the case, since adjacent O(1) species belong to different layers, this type of defect would considerably increase the interlayer binding.

In the context of the results summarised in Fig. 8, it is important to comment on the procedure employed to estimate the electron correlation in the system. As we have mentioned previously, the method is based on a density functional of the equilibrium HF electron density; the procedure has been shown to work in many recent solid-state applications (see for instance ref. 40 and 41). In all the above cases, however, correlation represented only a minor correction to the HF interaction, which seems not to be the case for the O(1)···O(1) interactions discussed above. We suggest that future studies of this system should aim at improving the estimate of the electron correlation; in particular it would seem desirable to include the effect of correlation in the SCF procedure, hence influencing the wavefunction and not only the total energy. Work is in progress to include this functionality in the program that we have employed. As a consequence, at the present stage we consider the HF results relating to the optimisation of the interlayer spacing as more reliable than those using correlation corrections, and we used the HF equilibrium value of the scaling factor X in the calculated data reported in Table 1.

One very important question that can be addressed in the light of the results reported here and in the previous section concerns why the tungsten analogue of the layered structure of MoO_3 has never been observed. One key factor in this respect appears to be the electrostatic repulsion between the facing O(1) species in adjacent layers, as clearly shown in Fig. 8. The higher degree of covalence that characterises MoO_3 contributes to reducing the ionic charge on the oxygens, including O(1), and therefore to reducing the electrostatic repulsion between layers. Indeed, we have already noted how strikingly low the net charge is on this species. The covalent contribution to the bonding is less pronounced for the less electronegative W atom; in a hypothetical layer structured WO_3 the layer–layer electrostatic repulsion would be much higher, thus stabilising the perovskite with respect to the layered polymorph.

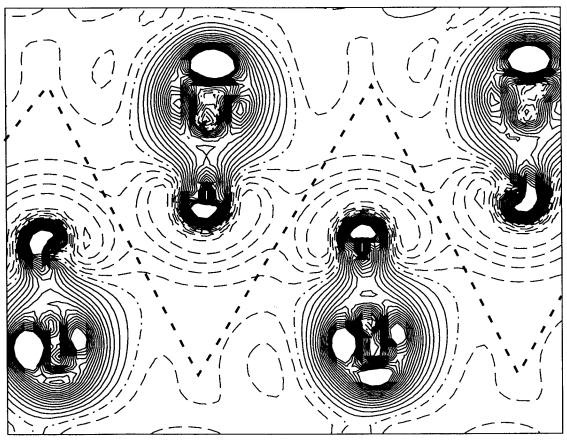

Fig. 8 Difference electron density map in the plane through the outermost molybdenyl groups [Mo—O(1)] in adjacent layers, showing the zip-like connection of layers and the short O(1)···O(1) equilibrium distance. The zigzag dashed line in the centre of the plot serves as a guideline to separate the molybdenyl groups belonging to each of the two facing layers.

Conclusions

Our calculations have given substantial insight into the relation between structure and bonding in α-MoO_3. In particular, we have shown that oxygens with a different coordination number behave as truly different chemical species in the solid; as a consequence the octahedron of oxygen ligands surrounding each Mo ion is highly distorted. The distortion is driven by the different balance of covalence and ionicity in the different Mo—O bonds. Both covalent and ionic contributions are important in the intralayer interactions; covalence, in particular, is the dominant force in the bonding between Mo and the singly coordinated oxygen, O(1). We identified the strongly bound Mo—O(1) pair as a molybdenyl group. The covalent contribution in the two shortest bonds of the MoO_6 octahedron is clearly seen and characterised from both charge density difference maps and population analyses. Interlayer forces are weak and Coulombic in nature. The stabilisation of the α-MoO_3 structure compared with the ReO_3 like structure adopted by WO_3 can be attributed to the greater degree of covalence in the former, which reduces the Coulomb repulsion between the molybdenyl groups which face each other in the interlayer region.

The results of the present quantum-mechanical *ab initio* calculations on α-MoO_3 have shown that the method is successful in modelling the geometry, including layer spacing, and the electronic structure of α-MoO_3. Further studies of the structure and bonding in complex transition-metal oxides are encouraged by the success of this work.

We are grateful to the Defence Research Agency (DRA) and to EPSRC for supporting this work. We would like to thank Dr. Richard Mortimer for useful discussions. F.C. acknowledges financial support from ICI Katalco and Molecular Simulations Inc. (MSI).

References

1 J. Haber and M. Wojciechowska, *Stud. Surf. Sci. Catal.*, 1995, **92**, 87.
2 M. C. Kim and K. L. Kim, *Korean J. Chem. Eng.*, 1996, **13**, 1.
3 B. S. Shin, S. Y. Lim and S. J. Choung, *Korean J. Chem. Eng.*, 1994, **11**, 254; H. Matralis, S. Theret, P. Bastians, M. Ruwet and P. Grange, *Appl. Catal. B*, 1995, **5**, 271.
4 S. H. Taylor, J. S. J. Hargreaves, G. J. Hutchings and R. W. Joyner, *Appl. Catal. A*, 1995, **126**, 287.
5 W. Grünert, A. Y. Stakheev, W. Mörke, R. Feldhaus, K. Anders, E. S. Shpiro and K. M. Minachev, *J. Catal.*, 1992, **135**, 269.
6 U. S. Ozkan, R. E. Gooding and B. T. Schilf, *ACS Symp. Ser.*, 1996, **638**, 178.
7 Y. M. Li and T. Kudo, *Sol. Energy Mater. Sol. Cells*, 1995, **39**, 179.
8 P. E. Sheehan and C. M. Lieber, *Science*, 1996, **272**, 1158.
9 C. Schlenker and J. Dumas, in *Crystal Chemistry and Properties of Materials with Quasi-One-Dimensional Structures*, ed. J. Rouxel, Reidel, Netherlands, 1986.
10 E. M. McCarron III, *J. Chem. Soc., Chem. Commun.*, 1986, 336.

11 J. B. Parise, E. M. McCarron III, R. Von Dreele and J. A. Goldstone, *Solid State Commun*., 1991, **93**, 193.
12 W. Biltz, G. A. Lehrer and K. Meisel, *Z. Anorg. Allg. Chem*., 1932, **207**, 113.
13 E. Salje, *Acta Crystallogr., Sect. B*, 1977, **33**, 547.
14 H. Brakken, *Z. Kristallogr*., 1931, **78**, 484.
15 N. Wooster, *Z. Kristallogr*., 1931, **80**, 504.
16 L. Kihlborg, *Ark. Kemi*, 1963, **21**, 357.
17 R. A. Wheeler, M.-H. Whangbo, T. Hughbanks, R. Hoffman, J. K. Burdett and T. A. Albright, *J. Am. Chem. Soc*., 1986, **108**, 2222.
18 F. Corà, A. Patel, N. M. Harrison, R. Dovesi and C. R. A. Catlow, *J. Am. Chem. Soc*., 1996, **118**, 12174.
19 M. G. Stachiotti, F. Corà, C. R. A. Catlow and C. O. Rodriguez, *Phys. Rev. B*, in press.
20 F. Corà, M. G. Stachiotti, C. R. A. Catlow and C. O. Rodriguez, *J. Phys. Chem*., in press.
21 S. V. Chernov, S. F. Ruzankin and A. L. Yakovlev, *J. Struct. Chem*., 1995, **36**, 918.
22 C. Pisani, R. Dovesi and C. Roetti, *Hartree–Fock Ab Initio Treatment of Crystalline Systems* (*Lecture Notes in Chemistry, Vol. 48*), Springer, Heidelberg, 1988.
23 R. Dovesi, V. R. Saunders and C. Roetti, CRYSTAL 92 User's manual, Gruppo di Chimica Teorica, Università di Torino, Turin, Italy, 1992.
24 J. P. Perdew, *Electronic Structure of Solids*, ed. P. Ziesche and H. Eschrig, Akademic Verlag, Berlin, 1991.
25 J. P. Perdew, J. A. Chevary, S. H. Vosko, K. A. Jackson, M. R. Pederson, D. J. Singh and C. Fiolhais, *Phys. Rev. B*, 1992, **46**, 6671.
26 H. J. Monkhorst and J. D. Pack, *Phys. Rev. B*, 1976, **13**, 5188.
27 P. J. Hay and W. R. Wadt, *J. Chem. Phys*., 1985, **82**, 270; 284; 299.
28 W. J. Hehre, L. Radom, P. V. R. Schleyer and J. A. Pople, *Ab Initio Molecular Orbital Theory*, Wiley, New York, 1986.
29 M. Causà, R. Dovesi, C. Pisani and C. Roetti, *Phys. Rev. B*, 1986, **33**, 1308.
30 R. Nada, C. R. A. Catlow, R. Dovesi and C. Pisani, *Phys. Chem. Miner*., 1990, **17**, 353.
31 P. D'arco, G. Sandrone, R. Dovesi, R. Orlando and V. R. Saunders, *Phys. Chem. Miner*., 1993, **20**, 407.
32 F. A. Cotton and G. Wilkinson, *Advanced Inorganic Chemistry*, Interscience, New York, 5th edn., 1988.
33 N. M. Harrison and V. R. Saunders, *J. Phys. Condens. Matter*, 1992, **4**, 3873.
34 N. M. Harrison, V. R. Saunders, E. Aprà, M. Causà and R. Dovesi, *J. Phys. Condens. Matter*, 1992, **4**, L261.
35 P. D'arco, M. Causà, C. Roetti and B. Silvi, *Phys. Rev. B*, 1993, **47**, 3522.
36 P. D. Fleischauer, *Thin Solid Films*, 1987, **154**, 309.
37 R. Orlando, R. Dovesi, C. Roetti and V. R. Saunders, *J. Phys. Condens. Matter*, 1990, **2**, 7769.
38 C. G. Granqvist, *Handbook of Inorganic Electrochromic Materials*, Elsevier, Amsterdam, 1995.
39 J. K. Burdett and S. A. Gramsch, *Inorg. Chem*., 1994, **33**, 4309.
40 M. Causà and A. Zupan, *Chem. Phys. Lett*., 1994, **220**, 145.
41 R. Dovesi, C. Roetti, C. Freyria-Fava, E. Aprà, V. R. Saunders and N. M. Harrison, *Phil. Trans. R. Soc. London, Ser. A*, 1992, **203**, 341.

Paper 6/07439A; *Received* 1*st November*, 1996